V European Conference on Computational Fluid Dynamics
ECCOMAS CFD 2010
J. C. F. Pereira and A. Sequeira (Eds)
Lisbon, Portugal,14-17 June 2010

NUMERICAL SIMULATION OF BLOOD FLOW USING GENERALIZED OLDROYD-B MODEL

Luboš Pirkl* **and Tomáš Bodnár***

*Czech Technical University, Faculty of Mechanical Engineering,
Department of Technical Mathematics

Karlovo Náměsti 13, 121 35 Prague 2, Czech Republic

e-mail: lubos.pirkl@seznam.cz

e-mail: bodnar@marian.fsik.cvut.cz

Key words: Computational Fluid Dynamics, Navier-Stokes equations, Non-Newtonian fluid, Shear-Thinnning model, Viscoelastic model, Blood flow, Oldroyd-B, Finite Volume Method

Abstract. *The paper presents a numerical simulation of blood flow using generalized viscoelastic model. Mathematical model is based on incompressible Navier-Stokes equations which are generalized to take into acount viscoelasticity and shear-thinning properties of blood flow. The numerical method used for solution of the governing system of equations is based on the Finite Volume discretization. The scheme uses central in space discretization of cell-centered type on structured grid. The steady solution is obtained by time-marching technique using artificial compressibility method.*

1 INTRODUCTION

This study presents a numerical simulation of blood flow using shear-thinning viscoelastic model.

Blood is a suspension of large number of formed elements ($cells$) in an aqueous polymer solution ($plasma$). There are three kinds of cells: Red blood cells (RBC) , white blood cells (WBC) and platelets. RBC has biconcave shape with diameter of about $7 \cdot 10^{-6}m$. The blood cells are present in a ratio of approximately 45% cells and 55% plasma. Plasma contains water (approximately 90-92% by weight), mineral ions such as K^+, Na^-, Cl^-, HCO_3^-, HPO_4^-, (approximately 1-2%) and the reminder (7%) are various proteins. The red blood cells have a tendency to attach themselves side by side to form what are described as rouleaux, resembling a stack of coins. The phenomena to form rouleaux is called *aggregation*. The attraction is attributed to charged groups on the surface of cells. The process is reversible and also depends on the presence fibrinogen and globulins. The red blood cells also can *deform* into a infinite variety of shapes without changing volume or surface area. All above mentioned properties of blood results in conclusions that blood can be described as a non-Newtonian (*shear-thinning*, *viscoelastic*) liquid.

The computational test case is based on two dimensional symmetric channel geometry imitating idealized blood vessel. The channel is either widened to simulate the vessel aneurysm, or is narrowed to simulate its stenosis. The aim of this study is to show the differences in solutions obtained by four types of models often used in blood flow simulations. These are the *Newtonian*, *Generalized Newtonian*, *Odroyd-B* and *Generalized Oldroyd-B* models.

2 MATHEMATICAL MODEL

Mathematical model is based on incompressible Navier-Stokes equations which are generalized to take into account viscoelasticity and shear-thinning properties of blood flow. The model used to capture viscoelastic properties of the blood flow is the generalized Oldroyd-B model. The numerical method used for solution of the governing system of equations is based on the Finite Volume discretization. The scheme uses central in space discretization of cell-centered type on structured grid. The steady solution is obtained by time-marching technique using artificial compressibility method. The governing system of equations is based on *Navier-Stokes* equations using *Johnson-Segalman* model for stress tensor. The system of equations can be written in the following general form:

$$\mathrm{div}\,\mathbf{u} = 0 \tag{1}$$

$$\rho\frac{\mathrm{d}\mathbf{u}}{\mathrm{d}t} = \mathrm{div}\mathbf{T} - \nabla p \tag{2}$$

$$\mathbf{T} + \lambda_1\frac{\delta\mathbf{T}}{\delta t} = 2\mu(\dot{\gamma})(\mathbf{D} + \lambda_2\frac{\delta\mathbf{D}}{\delta t}) \tag{3}$$

Here $\mathbf{T}$ is the stress tensor, $\mathbf{D}$ is symmetric part of the velocity gradient, $\dot{\gamma}$ is the shear rate and λ_1 and λ_2 denote the relaxation- resp. retardation time. Stress tensor $\mathbf{T}$ can be splitted into two parts:

$$
\begin{aligned}
\mathbf{T} &= \mathbf{T}_s + \mathbf{T}_e && (4)\\
\mathbf{T}_s &= 2\mu_s \mathbf{D} && (5)\\
\mathbf{T}_e + \lambda \frac{\delta \mathbf{T}}{\delta t} &= 2\mu_e \mathbf{D} && (6)\\
\mathbf{T_e} &= \begin{pmatrix} t_1 & t_2 & t_3 \\ t_2 & t_4 & t_5 \\ t_3 & t_5 & t_6 \end{pmatrix} && (7)
\end{aligned}
$$

where $\mathbf{T}_s$ is solvent part of stress tensor that corresponds to Stokes law for Newtonian fluid. $\mathbf{T}_e$ is viscoelastic (extra stress) part of stress tensor, the derivative expression $\frac{\delta}{\delta t}$ is *convected derivative*, which is for general quantity Q following:

$$
\left(\frac{\delta \mathsf{Q}}{\delta t}\right)_a = \dot{\mathsf{Q}} - \mathbf{W}\mathsf{Q} + \mathsf{Q}\mathbf{W} + a(\mathbf{D}\mathsf{Q} + \mathsf{Q}\mathbf{D}) \tag{8}
$$

2.1 Viscoelasticity contribution

Viscoelastic part of stress tensor $\mathbf{T}_e$ is a symmetric tensor of second order (as well as $\mathbf{T}$ and $\mathbf{T}_s$) therefore six components (in three dimensions) must be computed. Extra stress tensor can be evaluated from the following equation:

$$
\frac{\partial \mathbf{T}_e}{\partial t} + (\mathbf{u} \cdot \nabla)\mathbf{T}_e = \frac{2\mu_e}{\lambda}\mathbf{D} - \frac{1}{\lambda}\mathbf{T}_e + (\mathbf{W}\mathbf{T}_e - \mathbf{T}_e\mathbf{W}) - a(\mathbf{D}\mathbf{T}_e - \mathbf{T}_e\mathbf{D}) \tag{9}
$$

Where model constants are: $\lambda = 0.06s$. The derivative constant is $a = -1.0$ which leads to *Upper-convected* derivative and the model is called *Oldroyd-B* model. Tensors $\mathbf{D}$ & $\mathbf{W}$ are symmetric and antisymmetric parts of velocity gradient:

$$
\mathbf{D} = \frac{1}{2}\begin{pmatrix} 2\mathsf{u}_x & \mathsf{v}_x + \mathsf{u}_y & \mathsf{w}_x + \mathsf{u}_z \\ \mathsf{u}_y + \mathsf{v}_x & 2\mathsf{v}_y & \mathsf{w}_y + \mathsf{v}_z \\ \mathsf{u}_z + \mathsf{w}_x & \mathsf{v}_z + \mathsf{w}_y & 2\mathsf{w}_z \end{pmatrix} \tag{10}
$$

$$
\mathbf{W} = \frac{1}{2}\begin{pmatrix} 0 & \mathsf{v}_x - \mathsf{u}_y & \mathsf{w}_x - \mathsf{u}_z \\ \mathsf{u}_y - \mathsf{v}_x & 0 & \mathsf{w}_y - \mathsf{v}_z \\ \mathsf{u}_z - \mathsf{w}_x & \mathsf{v}_z - \mathsf{w}_y & 0 \end{pmatrix} \tag{11}
$$

More details about extra stress equation can be found e.g. in [3].

2.2 Shear-Thinning viscosity model

For evaluation of the variable viscosity the *Modified Cross Model* was used. The viscosity decreases from μ_0 to μ_∞ depending on the shear-rate. Model parameters are obtained by fitting an experimental data [6]. The Modified Cross Model is given by formula:

$$\mu(\dot{\gamma}) = \mu_\infty + (\mu_0 - \mu_\infty)\left[\frac{1}{[1+(\alpha\dot{\gamma})^m]^b}\right] \tag{12}$$

$$\dot{\gamma} = \frac{1}{2}\sqrt{\mathbf{D}:\mathbf{D}} = \frac{1}{2}\sqrt{\sum_{i,j} d_{i,j}^2} \tag{13}$$

$$\mathbf{D} = \frac{1}{2}\left(\frac{\partial \mathbf{u}_i}{\partial x_j} + \frac{\partial \mathbf{u}_j}{\partial x_i}\right) \tag{14}$$

where: $\mu_0 = 0.16\ Pa \cdot s$, $\mu_\infty = 0.0036\ Pa \cdot s$, $\alpha = 3.736\ s$, $m = 2.406$, $b = 0.254$. More information about blood viscosity models can be found e.g. in [6] or [5].

2.3 Model summary

Four different models were tested. The following table shows an overview of considered models:

Model name	Shear-Thinning	Viscoelasticity	μ_s	$\mathbf{T}_e$
Newtonian	no	no	μ_∞	**0**
Generalized Newtonian	**yes**	no	$\mu(\dot{\gamma})$	**0**
Oldroyd-B	no	**yes**	μ_∞	$\mathbf{T}_e$
Generalized Oldroyd-B	**yes**	**yes**	$\mu(\dot{\gamma})$	$\mathbf{T}_e$

Table 1: *Models overview*

All the models from the table (1) were tested for different flow rates, that correspond to the common blood flow rates in human body. Tested flow rates are $Q = 4,\ 2,\ 1\ \&\ 0.5\ cm^3\ /\ s$.

3 NUMERICAL MODEL

3.1 Governing equations

Incompressible Navier-Stokes equations can be rewritten in the following vector form:

$$P\boldsymbol{W}_t + \boldsymbol{F}_x + \boldsymbol{G}_y + \boldsymbol{H}_z = \boldsymbol{R}_x + \boldsymbol{S}_y + \boldsymbol{T}_z + \boldsymbol{f}_V \tag{15}$$

where: $\boldsymbol{W} = (\mathsf{p}, \mathsf{u}, \mathsf{v}, \mathsf{w})^T$ denotes the vector of unknowns, $\boldsymbol{F} = (\mathsf{u}, \mathsf{u}^2 + \mathsf{p}, \mathsf{uv}, \mathsf{uw})^T$, $\boldsymbol{G} = (\mathsf{v}, \mathsf{vu}, \mathsf{v}^2 + \mathsf{p}, \mathsf{vw})^T$ and $\boldsymbol{H} = (\mathsf{w}, \mathsf{wu}, \mathsf{wv}, \mathsf{w}^2 + \mathsf{p})^T$ are the vectors of inviscid (convective) fluxes, $\boldsymbol{R} = (0, \mathcal{K}(\mathsf{u}_x), \mathcal{K}(\mathsf{v}_x), \mathcal{K}(\mathsf{w}_x))^T$, $\boldsymbol{S} = (0, \mathcal{K}(\mathsf{u}_y), \mathcal{K}(\mathsf{v}_y), \mathcal{K}(\mathsf{w}_y))^T$ and $\boldsymbol{T} = (0, \mathcal{K}(\mathsf{u}_z), \mathcal{K}(\mathsf{v}_z), \mathcal{K}(\mathsf{w}_z))^T$ are the vectors of viscous (diffusive) fluxes, $P = diag(0, 1, 1, 1)$. Discretization of these equations is achieved using *Finite Volume Method* and *MacCormack scheme*, details can be found e.g. in [7] or [5]. For numerical solution were used *Artificial compressibility method*, see e.g. [7]. The discretization of equation (9) is analogous to the discretization of the basic equations.

3.2 Finite Volume Method

$$\frac{\boldsymbol{W}_{ijk}}{\partial t} = -\frac{1}{|D|}\left\{\underbrace{\oint_{\partial D}[\boldsymbol{F},\boldsymbol{G},\boldsymbol{H}]\cdot\boldsymbol{\nu}\,dS}_{\text{inviscid flux}} - \underbrace{\oint_{\partial D}[\boldsymbol{R},\boldsymbol{S},\boldsymbol{T}]\cdot\boldsymbol{\nu}\,dS}_{\text{viscous flux}} + \underbrace{\int_{D}\boldsymbol{f}_V\,dV}_{\text{external force}}\right\} \tag{16}$$

3.3 MacCormack Scheme

Explicit numerical scheme was used :

$$W_{i,j}^{n+\frac{1}{2}} = W_{i,j}^{n} - \frac{\Delta t}{|D_{i,j}|}\sum_{k=1}^{6}\{(F_k^n - R_k^n)\Delta x_k + (G_k^n - S_k^n)\Delta y_k + (H_k^n - T_k^n)\Delta z_k\} \tag{17}$$

$$\left(W_{i,j}^{n+1}\right) = \frac{1}{2}\Big(W_{i,j}^{n} + W_{i,j}^{n+\frac{1}{2}} - \frac{\Delta t}{|D_{i,j}|}\sum_{k=1}^{6}\{(F_k^{n+\frac{1}{2}} - R_k^{n+\frac{1}{2}})\Delta x_k + (G_k^{n+\frac{1}{2}} - S_k^{n+\frac{1}{2}})\Delta y_k + (H_k^{n+\frac{1}{2}} - T_k^{n+\frac{1}{2}})\Delta z_k\}\Big) \tag{18}$$

$$W_{i,j}^{n+1} = \left(W_{i,j}^{n+1}\right) + DW_{i,j}^{n} \tag{19}$$

where DW is stabilization term (one-dimensional case):

$$DW_i^n = \epsilon_2 \Delta x^3 \frac{d}{dx}|W_x|W_x\Big|_i^n + \epsilon_4 \Delta x^4 W_{xxxx}\Big|_i^n \tag{20}$$

more details can be found e.g. in [5].

4 TEST CASE SET-UP

4.1 Test geometries: axisymmertric stenosis & aneurysm

Both computational domains that were tested are straight channels with cosine narrowed/widened regions to imitate vessel stenosis/aneurysm. Channels are assumed to be two-dimensional with diameter $D = 2R = 6.2mm$:

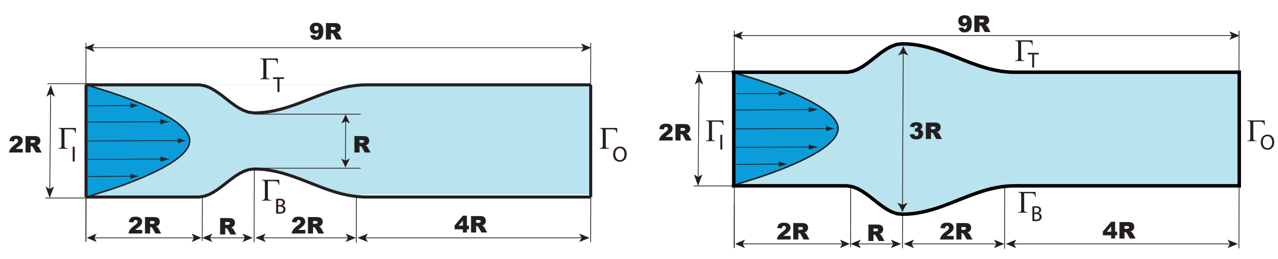

(a) Narrowed channel (stenosis) (b) Widened channel (aneurysm)

Figure 1: Test geometries

The numerical solver is three-dimensional, but in this study all the computations are 2D-like for simplicity. Parabolic velocity profile (corresponding to Newtonian flow) is prescribed at the inlet (mean value: $U_0 = 6.15 cm \cdot s^{-1}$) leading to Reynolds number: $Re = 100$. The Weissenberg number is $We = 0.6$. Outlet pressure is fixed to a constant. On the walls no-slip conditions are used for velocity and homogeneous Neumann condition for the pressure. For Oldroyd-B model variables ($\mathbf{T}e$) there is zero kept at the inlet and homogeneous Neumann condition at the walls and at the outlet. The computational grid has $80 \times 42 \times 1$ cells. The following set of figures shows comparison of axial velocity distribution in the narrowed channel for above described models:

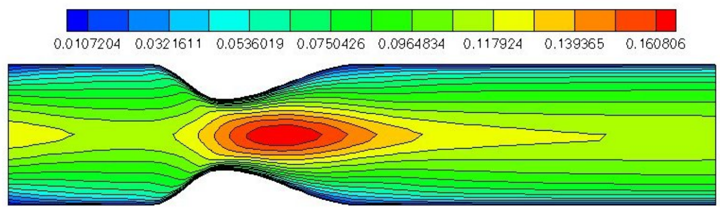

(a) Newtonian model

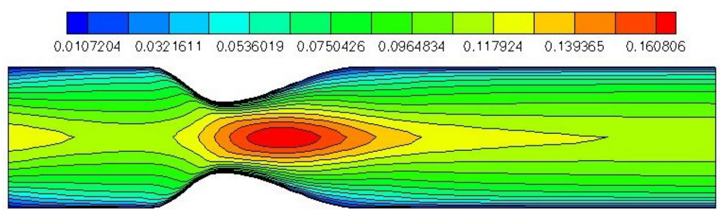

(b) Oldroyd-B model

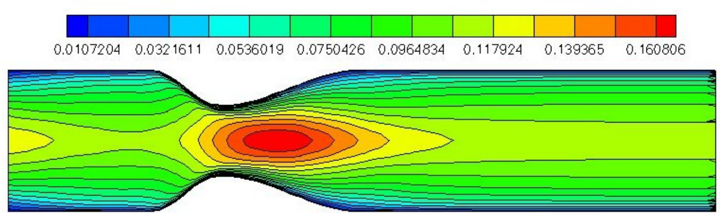

(c) Generalized Newtonian model

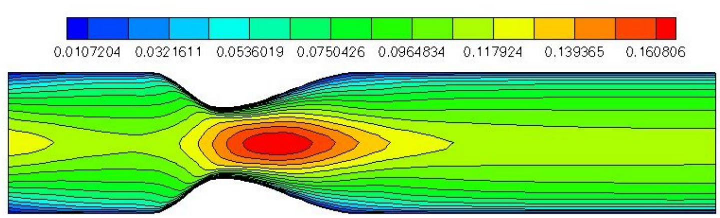

(d) Generalized Oldroyd-B model

Figure 2: Comparison of axial velocity distribution in the narrowed channel

Following figures show pressure and axial velocity distribution along the central axis of the channel:

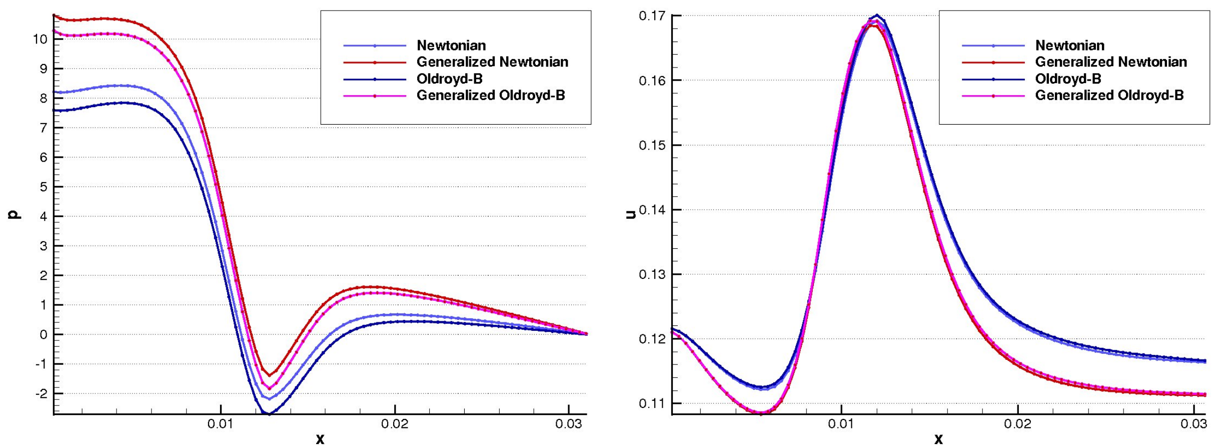

Figure 3: Narrowed channel, Pressure and axial velocity distribution along the centerline of the channel

In the following figure one can see wall shear stress distribution, here the wall shear stress is reduced to: $\tau_w = (\ \frac{du}{dy} \cdot \mu\ )\ |_{wall}$:

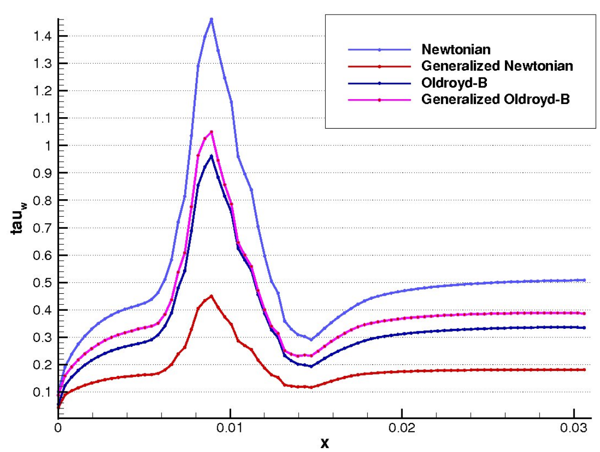

Figure 4: Narrowed channel, Wall shear stress distribution

All the above displayed results are of flow rate: $Q = 4\ cm^2/s$ according to [2].

Acknowledgement: The financial support for the present project was partly provided by the

Czech Science Foundation under the *Grant No.201/09/0917*, *The Grant Agency of the Academy of Sciences of the CR* under the *Grant No. IAA100190804* and by the Research Plan *MSM 6840770010* of the *Ministry of Education of the Czech Republic*.

5 CONCLUSIONS

- From the present results it is possible to interpret that the influence of shear-thinning behavior of blood on the main flow is considerably higher than the viscoelasticity for presented testcase. But one should keep in mind the complexity of the problem. While the variable viscosity (shear-thinning property) depends mainly on the ratio of the diameter of the channel and the flow rate, the viscoelasticity contribution is highly dependent on the channel geometry and velocity variability.
- The numerical method used to solve the governing equations seems to be sufficiently robust and efficient for the appropriate resolution of the given class of problems.

REFERENCES

[1] G. P. Galdi, R. Rannacher, A. M. Robertson, S. Turek : Hemodynamical Flows - Modeling, Analysis and Simulation, vol. 37 of Oberwolfach Seminars, Birkäuser, 2008.

[2] A. Leuprecht, K. Perktold : Computer methods in Biomechanics and Biomechanical Engineering 4, 149 - 163 (2001).

[3] T. Bodnár , A. Sequeira : Computational and Mathematical Methods in Medicine 9, 83 - 104 (2008).

[4] Bodnár T., Numerical Simulation of Flows and Pollution Dispersion in Atmospheric Boundary Layer, CTU Thesis, 2003

[5] Pirkl L., Numerical Simulation of Incompressible Flows with Variable Viscosity, Diploma Thesis, Czech Technical University of Prague, Faculty of Mechanical Engineering, Department of Technical Mathematics , Prague, 2007.

[6] Cho, Y.I., Kensey, K.R., Effects of Non-Newtonian Viscosity of Blood on Flows in Diseased Arterial Vessel, Part 1: Steady Flows, vol.28 (1991), pp. 41-262.

[7] Dvořák R., Kozel K., Matematické modelovaní v aerodynamice, Vydavatelství ČVUT, 1996.

[8] T. Bodnár , A. Sequeira : Numerical Study of the Significance of the Non-Newtonian Nature of Blood in Steady Flow Through a Stenosed Vessel. In: Advances in Mathematical Fluid Mechanics (edited by R. RANNACHER & A. SEQUEIRA), (pp. 83â104). Springer Verlag (2010)

[9] Bodnár T., Sequeira A., Pirkl, L. : Numerical Simulations of Blood Flow in a Stenosed Vessel under Different Flow Rates using a Generalized Oldroyd - B Model In: Numerical Analysis and Applied Mathematics, Vols 1 and 2. Melville, New York: American Institute of Physics, 2009, vol. 2, p. 645-648. ISBN 978-0-7354-0709-1.